Fluid Antenna Systems With Terrestrial Interference for Countering UAV Covert Communications

Jin Yao, Hui Zhao, Rui Zhang, and Gaofeng Pan, *Senior Member, IEEE*

***Abstract*—This paper studies covert communications in the presence of an unmanned aerial vehicle (UAV) acting as an aerial warden, where a terrestrial transmitter communicates with a legitimate terrestrial receiver under ground interference. To enhance transmission reliability, the legitimate receiver employs a fluid antenna (FA) with port selection based on the maximum signal-to-interference-plus-noise ratio (SINR). The UAV adopts an energy-detection-based hypothesis test to detect the covert transmission. Closed-form expressions for the false alarm and missed detection probabilities are derived, based on which the covertness outage probability (COP) is characterized. To tackle the analytical challenges introduced by spatially correlated FA channels, an eigenvalue-based weighted approximation is adopted to evaluate the outage probability at the legitimate receiver. Based on the derived outage and missed detection probability expressions, the success probability of covert communications is further characterized. Numerical results demonstrate that the proposed FA-assisted scheme significantly improves covert communications, and the eigenvalue-based weighted approximation remains highly accurate under various system parameter settings.**

***Index Terms*—Covert communications, fluid antenna, UAV and terrestrial interference.**

I. Introduction

Movable antennas (MAs) have recently attracted considerable attention due to their ability to dynamically reconfigure antenna positions and exploit location-dependent channel fluctuations for improved communication performance. Among the various MA architectures, fluid antenna (FA) systems have emerged as a particularly promising solution [1]–[3]. By dynamically selecting the optimal antenna port from a set of closely spaced positions, the FA can effectively combat deep fading and severe interference without relying on conventional antenna arrays, making it particularly attractive for size- and hardware-constrained wireless devices.

Covert communications have attracted significant attention as a means of enabling wireless transmissions that remain undetectable to adversaries or wardens, thereby providing a higher level of security beyond conventional cryptographic approaches [4], especially in the presence of increasingly powerful aerial wardens such as unmanned aerial vehicles (UAVs) [5], which can exploit nearly unobstructed wireless channels to conduct more effective surveillance and detection. While covert communications have been extensively studied in fixed-antenna systems, *the application of FA systems in covert communications remains largely unexplored*. Several preliminary studies along this line can be found in [6], [7]. From a fundamental perspective, the inherent port diversity of FA provides a new degree of freedom for enhancing the reliability of covert links, which in turn allows the transmit power to be reduced while maintaining a preset outage performance.

In practical wireless environments, terrestrial interference is ubiquitous due to the increasing scarcity of spectrum resources and the coexistence of heterogeneous wireless systems over shared frequency bands. As a result, both the legitimate receiver and the potential warden are inevitably affected by unintended interference from surrounding transmitters. Existing studies on covert communications assisted by FA typically neglect the presence of terrestrial interference (e.g., [6], [7]).

The analysis of FA systems is fundamentally challenging due to the strong spatial correlation among the wireless channels corresponding to different antenna ports [8]–[11]. The introduction of terrestrial interference further aggravates this difficulty, since the received signal-to-interference-plus-noise ratio (SINR) involves the ratio of correlated random processes associated with the desired and interfering links [12]–[16]. For key performance metrics such as the outage probability (OP), simple and tractable closed-form expressions are generally unavailable in such interference-limited and correlation-dominated scenarios. Although interference complicates the analysis, FA systems can achieve *sustained* outage performance improvements with an increasing number of ports for a fixed FA size [12]–[14], *effectively overcoming the saturation bottleneck encountered in interference-free cases*.

These observations motivate us to investigate FA-assisted covert communications in the presence of terrestrial interference and an aerial warden (e.g., UAV). The main contributions of this work are summarized as follows. i) Closed-form expressions for the false alarm probability and the missed detection probability at the UAV warden are derived, based on which the covertness outage probability (COP) is characterized. ii) To overcome the analytical intractability caused by the strong spatial correlation among FA ports, an eigenvalue-based weighted approximation is developed to evaluate the OP at the legitimate receiver. iii) By jointly considering the detectability at the UAV and the outage performance at the legitimate receiver, the success probability of covert communications is further characterized. Numerical results demonstrate that the proposed FA-assisted scheme significantly enhances covert transmission performance, while the proposed approximation remains highly accurate under various system parameter settings.

Paper Structure: Section II presents the system model and the considered performance metrics. Section III focuses on the detection performance analysis at the UAV warden. Section IV

This research was supported by the Science and Technology Research Program of Chongqing Municipal Education Commission (Grant No. KJQN202503305). The work of Hui Zhao was supported by the Huawei France-funded Chair toward Future Wireless Networks.

Jin Yao is with the Chongqing City Management University, 401331 Chongqing, China (email: 13983816609@163.com).

Hui Zhao is with the Communication Systems Department, EURECOM, 06410 Sophia Antipolis, France (email: hui.zhao@eurecom.fr).

Rui Zhang and Gaofeng Pan are with the School of Cyberspace Science and Technology, Beijing Institute of Technology, 100081 Beijing, China (email: rui.zhang@bit.edu.cn; gfpan@bit.edu.cn).

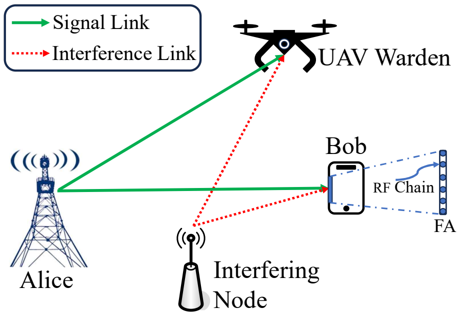

Fig. 1: FA-assisted covert communication system with a terrestrial interferer and an aerial UAV warden.

investigates the outage performance at the legitimate receiver and further characterizes the success probability of covert communications. Numerical results are provided in Section V, while Section VI concludes the paper.[1]

II. System Model

As shown in Fig. 1, we consider a covert communication scenario consisting of a terrestrial transmitter (Alice), a legitimate terrestrial receiver (Bob), a terrestrial interfering node, and an UAV acting as an aerial warden. All nodes are equipped with a single antenna, while Bob is further equipped with a FA with a single radio frequency (RF) chain [12]–[14].

A. UAV Detection

Alice transmits a sequence of K information symbols denoted by $\mathbf{x} = [x_1, x_2, \ldots, x_K]^T$ with unit average power, i.e., $\mathbb{E}\{|x_k|^2\} = 1$. The terrestrial interfering node simultaneously transmits an independent jamming signal. Let P_a and P_j denote the transmit powers of Alice and the interfering node, respectively. The wireless channel from Alice to the UAV is denoted by h_{au}, and the wireless channel from the terrestrial interfering node to the UAV is denoted by h_{ju}. The received signal at the UAV is of the form

$$y_u[k] = \begin{cases} \sqrt{P_j}\, h_{ju}\, s_j[k] + n_u[k], & \mathcal{H}_0, \\ \sqrt{P_a}\, h_{au}\, x[k] + \sqrt{P_j}\, h_{ju}\, s_j[k] + n_u[k], & \mathcal{H}_1, \end{cases} \tag{1}$$

where $s_j[k]$ denotes the jamming symbol with unit average power, $n_u[k]$ denotes the additive white Gaussian noise (AWGN) at the UAV with variance σ_u^2, and $\mathcal{H}_0$ and $\mathcal{H}_1$ denote the hypotheses that Alice is silent and active, respectively.

The UAV adopts an energy-detection-based hypothesis test by comparing the average received signal power with a detection threshold ζ, i.e.,

$$P_r \triangleq \frac{1}{K} \sum_{k=1}^{K} |y_u[k]|^2 \underset{\mathcal{H}_0}{\overset{\mathcal{H}_1}{\gtrless}} \zeta. \tag{2}$$

[1] *Notations.* We use $\mathbb{C}$ to denote the set of complex numbers, and use $|\cdot|$ to represent the magnitude of a complex number. $\mathbb{E}\{\cdot\}$ denotes the expectation operator. For a matrix $\mathbf{A}$, $\mathbf{A}^T$, $\mathbf{A}^*$ and $\mathbf{A}^H$ represent its non-conjugate transpose, element-wise conjugate and conjugate transpose, respectively. $\mathbf{0}_N$ and $\mathbf{I}_N$ denote the $N \times 1$ all-zero vector and the $N \times N$ identity matrix, respectively. Moreover, $\mathcal{CN}(\mathbf{0}_N, \mathbf{I}_N)$ denotes the N-dimensional standard complex Gaussian distribution.

According to the above detection rule, the false alarm probability and the missed detection probability are defined as

$$P_{\mathrm{F}}(\zeta) \triangleq \Pr\left\{P_r > \zeta \,\middle|\, \mathcal{H}_0\right\}, \tag{3}$$

$$P_{\mathrm{M}}(\zeta) \triangleq \Pr\left\{P_r \leq \zeta \,\middle|\, \mathcal{H}_1\right\}. \tag{4}$$

Based on $P_{\mathrm{F}}(\zeta)$ and $P_{\mathrm{M}}(\zeta)$, the COP is defined as

$$P_{\mathrm{co}}(\zeta) \triangleq 1 - \big(P_{\mathrm{F}}(\zeta) + P_{\mathrm{M}}(\zeta)\big). \tag{5}$$

B. Signal Model at Bob

Bob is equipped with a FA with N ports. The channel gain from Alice to the ℓ-th FA port of Bob and from the terrestrial interfering node to the ℓ-th port of Bob are denoted by $h_{ab}^{(\ell)}$ and $h_{jb}^{(\ell)}$, respectively, for $\ell = 1, 2, \ldots, N$.

When Alice is transmitting, the received signal at the ℓ-th FA port of Bob is given by

$$y_b^{(\ell)} = \sqrt{P_a}\, h_{ab}^{(\ell)} x + \sqrt{P_j}\, h_{jb}^{(\ell)} s_j + n_b^{(\ell)}, \tag{6}$$

where $n_b^{(\ell)}$ denotes the AWGN at the ℓ-th port with variance σ_b^2. Accordingly, the instantaneous SINR at the ℓ-th port is

$$\gamma_b^{(\ell)} = \frac{P_a |h_{ab}^{(\ell)}|^2}{P_j |h_{jb}^{(\ell)}|^2 + \sigma_b^2} \overset{(a)}{\simeq} \frac{P_a |h_{ab}^{(\ell)}|^2}{P_j |h_{jb}^{(\ell)}|^2}. \tag{7}$$

where the step (a) used the signal-to-interference ratio (SIR) approximation by assuming the typical interference-limited regime in FA systems, in which the noise power is negligible compared to the interference power (cf. [12]–[14]).

Remark 1: The SIR expression in (7) can also be interpreted as the SIR of a typical user in a two-user fluid antenna multiple access (FAMA) system [14]. Moreover, it can be readily extended to fast FAMA in the presence of multiple interfering users [12], where P_j accounts for the cumulative interference power contributed by all interfering users.

Bob performs FA port selection based on the maximum SINR criterion (cf. [12]–[14]), i.e., $\ell^\star = \arg\max_{\ell \in \{1,\ldots,N\}} \gamma_b^{(\ell)}$, and the resulting effective SINR at Bob is given by[2]

$$\gamma_b = \max_{\ell \in \{1,\ldots,N\}} \gamma_b^{(\ell)}. \tag{8}$$

For a given target transmission rate $R_{\mathrm{th}} = \log_2(1 + \gamma_{\mathrm{th}})$, an outage event occurs when the instantaneous rate at Bob is below the target rate. Accordingly, the OP at Bob is defined as

$$P_{\mathrm{out}} \triangleq \Pr\{\gamma_b < \gamma_{\mathrm{th}}\} \simeq P_{\mathrm{out}}^{\mathrm{SIR}}, \tag{9}$$

where $P_{\mathrm{out}}^{\mathrm{SIR}}$ denotes the *SIR-based OP* based on the approximation in (7), which provides a tight characterization under typical interference-limited conditions [12]–[14].

In covert communications, a successful transmission from Alice to Bob requires that the UAV warden fails to detect Alice's transmission and that Bob is able to decode the message reliably. Therefore, the success probability of covert communications is defined as

$$P_{\mathrm{suc}} = P_{\mathrm{M}}(\zeta) \times \big(1 - P_{\mathrm{out}}\big), \tag{10}$$

where $P_{\mathrm{M}}(\zeta)$ denotes the missed detection probability in (4).

[2] Recent FA hardware prototypes have demonstrated very fast port switching capabilities [1], suggesting that the selected SINR in (8) can serve as a reasonable performance benchmark. However, the analysis of port-switching overhead and channel measurement is beyond the scope of this work.

C. Channel Models

Both the Alice-to-UAV channel and the jammer-to-UAV channel are modeled as independent Nakagami-m fading channels to capture the potential presence of line-of-sight (LoS) components in air-ground links [17]. The Alice-to-UAV and jammer-to-UAV links are hereafter referred to as the first and second air-ground links, respectively. The channel power gain $|h_{au}|^2$ follows a Gamma distribution with shape parameter m_1 and scale parameter Ω_1, while the channel power gain $|h_{ju}|^2$ follows a Gamma distribution with shape parameter m_2 and scale parameter Ω_2.

Denote $\mathbf{h}_{ab} \triangleq [h_{ab}^{(1)}, \ldots, h_{ab}^{(N)}]^T$ and denote $\mathbf{h}_{jb} \triangleq [h_{jb}^{(1)}, \ldots, h_{jb}^{(N)}]^T$. For each port, the small-scale fading channels are modeled as Rayleigh fading, such that the corresponding channel power gains $|h_{ab}^{(\ell)}|^2$ and $|h_{jb}^{(\ell)}|^2$ follow exponential distributions with unit mean. Due to the close placement among the FA ports, the channel coefficients across different ports are spatially correlated. Let $\mathbf{J} \in \mathbb{C}^{N\times N}$ denote the spatial correlation matrix among the N ports. Then, the channel vectors can be expressed as [2], [9]

$$\mathbf{h}_{ab} = \mathbf{J}^{1/2}\mathbf{z}, \qquad \mathbf{h}_{jb} = \mathbf{J}^{1/2}\mathbf{z}', \tag{11}$$

where $\mathbf{z}, \mathbf{z}' \sim \mathcal{CN}(\mathbf{0}_N, \mathbf{I}_N)$ are independent random vectors.

III. UAV Detection Analysis

In this section, we analyze the detection performance at the UAV. As discussed in Section II, the UAV adopts an energy-detection-based test by comparing the average received signal power with a detection threshold ζ. For tractability, we consider that the number of observed symbols K is sufficiently large so that, by invoking the strong law of large numbers, the empirical average converges to the corresponding received power [4]. The received power in (2) can be simplified as[3]

$$P_r = \begin{cases} P_j|h_{ju}|^2 + \sigma_u^2, & \mathcal{H}_0, \\ P_a|h_{au}|^2 + P_j|h_{ju}|^2 + \sigma_u^2, & \mathcal{H}_1. \end{cases} \tag{12}$$

In the following, we derive the missed detection probability and the false alarm probability based on the above power model.

Lemma 1: For positive integer Nakagami-m fading shape parameters m_1 and m_2, the missed detection probability at the UAV for a given detection threshold ζ is given by

$$P_{\mathrm{M}}(\zeta) = \begin{cases} 0, & \zeta \le \sigma_u^2, \\ P'_{\mathrm{M}}(\zeta), & \zeta > \sigma_u^2, \end{cases} \tag{13}$$

where $P'_{\mathrm{M}}(\zeta)$ is defined as

$$P'_{\mathrm{M}}(\zeta) \triangleq \frac{\Upsilon\left(m_2, \dfrac{T}{P_j\Omega_2}\right)}{\Gamma(m_2)} - \frac{e^{-T/(P_a\Omega_1)}}{\Gamma(m_2)\Omega_2^{m_2}} \sum_{n=0}^{m_1-1} \frac{1}{n!\,(P_a\Omega_1)^n} \sum_{k=0}^{n} \binom{n}{k} T^{\,n-k}(-P_j)^k \frac{\Upsilon(m_2+k,\, \beta T/P_j)}{\beta^{\,m_2+k}}, \tag{14}$$

where $T \triangleq \zeta - \sigma_u^2$ and $\beta \triangleq \frac{1}{\Omega_2} - \frac{P_j}{P_a\Omega_1}$. In the above, $\Upsilon(\cdot,\cdot)$ and $\Gamma(\cdot)$ denote the lower incomplete Gamma function and the Gamma function [18], respectively.

Proof: As shown in (12), the received power at the UAV under $\mathcal{H}_1$ is $P_r = P_a|h_{au}|^2 + P_j|h_{ju}|^2 + \sigma_u^2$. For $\zeta \le \sigma_u^2$, we have $P_r > \zeta$ almost surely and hence $P_{\mathrm{M}}(\zeta) = 0$. For $\zeta > \sigma_u^2$, the missed detection probability can be written as

$$\begin{aligned} P_{\mathrm{M}}(\zeta) &= \Pr\left\{P_a|h_{au}|^2 + P_j|h_{ju}|^2 \le T\right\} \\ &= \int_0^{T/P_j} \Pr\left\{|h_{au}|^2 \le \frac{T - P_j y}{P_a}\right\} f_{|h_{ju}|^2}(y)\,\mathrm{d}y, \end{aligned} \tag{15}$$

where $f_{|h_{ju}|^2}(\cdot)$ denotes the PDF of $|h_{ju}|^2$. For positive integer m_1, the cumulative distribution function (CDF) of $|h_{au}|^2$ can be expressed as

$$\Pr\{|h_{au}|^2 \le x\} = 1 - \exp\left(-\frac{x}{\Omega_1}\right) \sum_{n=0}^{m_1-1} \frac{1}{n!}\left(\frac{x}{\Omega_1}\right)^n. \tag{16}$$

Substituting this expression into (15) and separating the integral into two parts yields

$$P_{\mathrm{M}}(\zeta) = \Pr\left\{|h_{ju}|^2 \le \frac{T}{P_j}\right\} - \mathcal{J}(T), \tag{17}$$

where $\mathcal{J}(T)$ collects the terms involving the exponential series. By expanding the polynomial term using the binomial theorem and utilizing the integral identity in [18, Eq. (3.351.1)], the term $\mathcal{J}(T)$ can be written in closed form as the double summation in (14). This completes the proof. ■

Lemma 2: For a given detection threshold ζ, the false alarm probability at the UAV is given by

$$P_{\mathrm{F}}(\zeta) = \begin{cases} 1, & \zeta \le \sigma_u^2, \\ 1 - \dfrac{1}{\Gamma(m_2)}\Upsilon\left(m_2, \dfrac{T}{P_j\Omega_2}\right), & \zeta > \sigma_u^2. \end{cases} \tag{18}$$

Proof: The proof directly follows from the CDF of $|h_{ju}|^2$. ■

Corollary 1: The COP at the UAV is given by $P_{\mathrm{co}}(\zeta) = 1 - \big(P_{\mathrm{F}}(\zeta) + P_{\mathrm{M}}(\zeta)\big)$, where $P_{\mathrm{F}}(\zeta)$ and $P_{\mathrm{M}}(\zeta)$ are given in (18) and (13), respectively.

Proof: The proof follows directly from the definition of the COP in (5), together with the results in Lemmas 1 and 2. ■

IV. Outage and Success Probability Analysis

In this section, we analyze the outage performance at the legitimate receiver and the resulting success probability of covert communications.

Let X and Y be two independent exponential random variables with unit mean. Define the random variable $Z \triangleq X/Y$. Then, the CDF of Z is expressed as follows.

Proposition 1: The CDF of Z is of the form

$$F_Z(z) = \Pr\{Z \le z\} = \frac{z}{1+z}, \quad z \ge 0. \tag{19}$$

Proof: By definition, the CDF of Z can be written as

$$F_Z(z) \overset{(a)}{=} \int_0^{\infty} (1 - \exp(-zy))\exp(-y)\mathrm{d}y = \frac{z}{1+z}, \tag{20}$$

where (a) follows from using the distribution functions of X and Y, and which completes the proof. ■

[3] Large observation lengths are commonly assumed in the literature (cf. [4] and the references therein) to facilitate analysis. While the finite-K regime is also of interest, it is left for future investigation.

Let $\rho \triangleq P_a/P_j$. Then, γ_b in (7) can be written as

$$\gamma_b \simeq \rho \max_{\ell\in\{1,\ldots,N\}} Z'_\ell, \tag{21}$$

where each ratio $Z'_\ell \triangleq |h_{ab}^{(\ell)}|^2/|h_{jb}^{(\ell)}|^2$ follows the distribution characterized in Proposition 1.

To obtain a tractable expression, we adopt an eigenvalue-based weighted approximation. Let $\lambda_1,\ldots,\lambda_M$ denote the $M = \mathrm{Rank}(\mathbf{J})$ non-zero eigenvalues of $\mathbf{J}$. We extend the approximation framework in [11], which was initially designed for point-to-point FA systems, to the more general scenario involving external interference. Specifically, the correlated set $\{Z'_\ell\}$ is approximated by a set of M independent random variables $\{\lambda_m Z_m\}_{m=1}^M$, where $\{Z_m\}$ are i.i.d. and each Z_m has the same distribution as Z in Proposition 1. Under this approximation, (21) can be rewritten as

$$\gamma_b \approx \rho \max_{m\in\{1,\ldots,M\}} \lambda_m Z_m. \tag{22}$$

Lemma 3: Under the eigenvalue-based weighted approximation, the SIR-based OP at Bob in (9) is approximated as

$$P_{\mathrm{out}}^{\mathrm{SIR}} \approx \prod_{m=1}^{M} \frac{\gamma_{\mathrm{th}}}{\gamma_{\mathrm{th}} + \rho\lambda_m}. \tag{23}$$

Proof: Using (22), the SIR-based OP can be approximated as

$$P_{\mathrm{out}}^{\mathrm{SIR}} \approx \Pr\Big\{\rho \max_m \lambda_m Z_m < \gamma_{\mathrm{th}}\Big\} = \prod_{m=1}^{M} \Pr\Big\{Z_m < \frac{\gamma_{\mathrm{th}}}{\lambda_m \rho}\Big\}, \tag{24}$$

where the last equality follows from the independence of $\{Z_m\}$. By substituting the CDF of Z in (19) into (24), (23) is readily obtained, which completes the proof. ■

Remark 2: The performance analysis of FAMA has long been a technically challenging problem. The resulting OP expressions in existing studies typically involve complicated multiple integrals (e.g., [12]–[14]) or rely on copula-based approaches for approximation [19]. Compared with these existing results, Lemma 3 leads to a remarkably simple OP expression for the widely studied FAMA systems. It is expressed purely in terms of elementary functions, which makes it attractive for both theoretical analysis and practical system design. The numerical results in Fig. 2 further verify the high accuracy of Lemma 3.

Remark 3: The proposed approximation does not rely on any specific FA structure. Instead, it depends solely on the non-zero eigenvalues of the correlation matrix $\mathbf{J}$, which fully characterize the spatial correlation among the FA port channels. This makes the approximation broadly applicable to a wide variety of FA implementations. Further discussion on the eigenvalue properties of $\mathbf{J}$ can be found in [15].

Corollary 2: The success probability of covert communications is given by $P_{\mathrm{suc}} \approx P_{\mathrm{M}}(\zeta) \times \left(1 - P_{\mathrm{out}}^{\mathrm{SIR}}\right)$, where $P_{\mathrm{M}}(\zeta)$ and $P_{\mathrm{out}}^{\mathrm{SIR}}$ are given in Lemmas 1 and 3, respectively.

Proof: The proof is readily obtained by combining the definition in (10) with the results in Lemmas 1 and 3. ■

The developed outage analysis is based on the interference-limited assumption. Since SINR does not exceed SIR, the resulting analytical success probability serves as an upper bound on the true success probability, becoming tight when

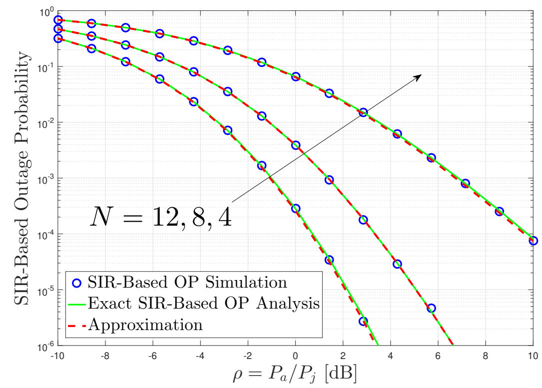

Fig. 2: SIR-based outage probability versus ρ for $W = 2$ and $P_j = 0$ dB.

interference dominates noise. Moreover, interference-limited operation is common in practical wireless systems, where the benefits of FA become more evident [12], [13].

V. Numerical Results

In this section, we present numerical results to validate the analytical expressions and to illustrate the performance of FA-assisted covert communications. Unless otherwise stated, we assume that $\sigma_u^2 = \sigma_b^2 = 0$ dB and set $\gamma_{\mathrm{th}} = 1$. All simulation results are averaged over 10^7 Monte Carlo realizations.[4]

A. Simplified Propagation Scenarios

For the FA configuration, we adopt the optimal constant inter-port correlation model for a linear FA of length W wavelengths, where any two FA ports share a common correlation coefficient μ, given by [20, Eq. (4)]

$$\mu^2 \triangleq \left| \frac{2}{N(N-1)} \sum_{k=1}^{N-1} (N-k)\, J_0\!\left(\frac{2\pi k W}{N-1}\right) \right|, \tag{25}$$

where $J_0(\cdot)$ denotes the zeroth-order Bessel function of the first kind [18]. Under this optimal correlation structure, the (k_1,k_2)-th entry of the correlation matrix $\mathbf{J} \in \mathbb{C}^{N\times N}$ is given by $[\mathbf{J}]_{k_1,k_2} = 1$ for $k_1 = k_2$ and $[\mathbf{J}]_{k_1,k_2} = \mu^2$ for $k_1 \neq k_2$. Under the optimal constant inter-port correlation model, the exact SIR-based OP expression was derived in [13, Thm. 2], and the result is reproduced in (26), shown at the top of the next page, where $c \triangleq \frac{\mu}{\sqrt{1-\mu^2}}$, $\gamma \triangleq \frac{\gamma_{\mathrm{th}}}{\rho}$, and $Q_\cdot(\cdot)$ and $I_\cdot(\cdot)$ denote the Marcum Q-function and the modified Bessel function of the first kind [18], respectively. In Fig. 2, we also include (26), labeled as *Exact SIR-Based OP Analysis*, for direct comparison with the proposed approximation in Lemma 3.

Fig. 2 plots the SIR-based OP versus $\rho = P_a/P_j$ with $W = 2$ for different N. It is observed that the proposed approximation in Lemma 3 closely matches the exact benchmark (26) across the considered ρ range and for all shown values of N, and it also aligns well with the Monte Carlo results. These results validate that the derived approximation provides a highly accurate yet

[4] Due to space limitations, we only briefly discuss the variation of the COP with respect to the detection threshold ζ. Numerical results indicate that the COP is a *unimodal* function of ζ. Moreover, the analytical expressions derived in Corollary 1 closely match the Monte Carlo simulation results, thereby validating the accuracy of the proposed COP characterization.

$$P_{\text{out}}^{\text{SIR}} = \frac{1}{4}\int_0^\infty\int_0^\infty \exp\left(-\frac{r+\tilde{r}}{2}\right)\left[Q_1\left(c\sqrt{\frac{\gamma\tilde{r}}{\gamma+1}},\ c\sqrt{\frac{r}{\gamma+1}}\right) - \frac{1}{\gamma+1}\exp\left(-\frac{c^2}{2}\frac{\gamma\tilde{r}+r}{\gamma+1}\right) I_0\left(c^2\frac{\sqrt{\gamma r\tilde{r}}}{\gamma+1}\right)\right]^N \mathrm{d}r\mathrm{d}\tilde{r} \quad (26)$$

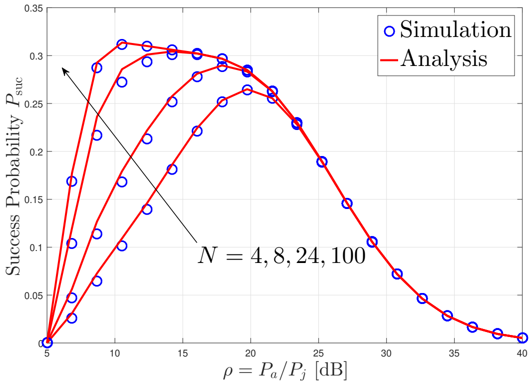

Fig. 3: Success probability versus ρ for $P_j = 20$ dB, $W = 1$, $m_1 = 2$, $m_2 = 3$, $\Omega_1 = m_1^{-1}$, $\Omega_2 = m_2^{-1}$ and optimized ζ for COP.

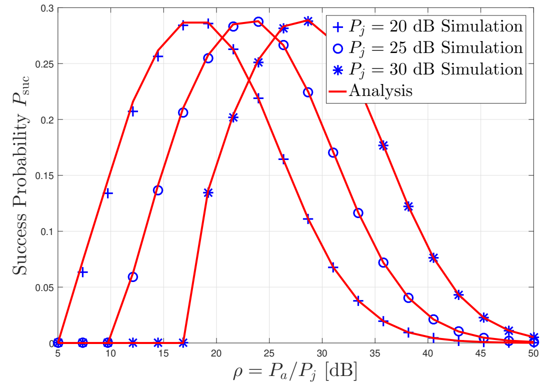

Fig. 4: Success probability versus ρ for $W = 1$, $N = 8$, $m_1 = 2$, $m_2 = 3$, $\Omega_1 = m_1^{-1}$, $\Omega_2 = m_2^{-1}$ and optimized ζ for COP.

much more tractable characterization of the outage performance, avoiding the computational burden associated with the double-integral evaluation.

Fig. 3 illustrates the success probability of covert communications as a function of $\rho = P_a/P_j$ for different numbers N, where the optimal detection threshold $\zeta^\star$ is adopted for COP at the UAV. As ρ increases, the success probability initially improves due to the enhanced reliability of the Alice–Bob link. However, further increasing ρ leads to a performance degradation, since stronger transmissions from Alice become more detectable at the UAV, resulting in a reduced missed detection probability. This highlights the fundamental tradeoff between transmission reliability and covertness. Increasing N enhances the *maximum* success probability and lowers the required transmit power at Alice. This is because a larger number of FA ports provides enhanced spatial diversity at Bob through FA port selection, which effectively reduces the OP.

Fig. 4 illustrates the success probability as a function of $\rho = P_a/P_j$ for different terrestrial interference power levels P_j, where the detection threshold ζ is optimized to maximize the COP. It is observed that the success probability exhibits a unimodal behavior with respect to ρ for all considered values of P_j. Moreover, increasing P_j shifts the optimal operating point toward larger values of ρ, indicating that stronger terrestrial interference necessitates a higher transmit power at Alice to sustain the optimal covert performance.[5] Simulations are conducted using the exact SINR in evaluating the OP in Figs. 3 and 4. The close agreement between the analytical results and the simulation outcomes further validates the accuracy of Corollary 2 in practical interference-limited scenarios.

B. Realistic Propagation Scenarios

To further validate the developed analytical framework under practical propagation environments, we consider a realistic air-ground channel model in which both the fading severity and the large-scale attenuation depend on the elevation angle of the ground node with respect to the UAV. Specifically, the Nakagami-m shaping parameter m_i $(i \in \{1,2\})$ is [17]

$$m_i = c_1 \exp(c_2\theta_i), \quad (27)$$

where $\theta_i = \arctan\left(\frac{h}{d_i}\right)$ denotes the elevation angle of the i-th air-ground link, h is the UAV altitude, d_i is the corresponding horizontal distance, and c_1 and c_2 are environment-dependent constants. When $\theta_i \to 0$, the UAV is located close to the ground plane, and we set $c_1 = 1$ such that the channel reduces to Rayleigh fading, i.e., $m_i = 1$. Accordingly, the scale parameter of the corresponding air-ground link is

$$\Omega_i = m_i^{-1} D_i^{-\alpha_i}, \quad (28)$$

where D_i denotes the slant distance between the UAV and the corresponding ground node, and α_i is the path-loss exponent, which is given by [17]

$$\alpha_i = \alpha_L^{(i)}\chi_L^{(i)} + \left(1-\chi_L^{(i)}\right)\alpha_{NL}^{(i)}, \quad (29)$$

where $\alpha_L^{(i)}$ and $\alpha_{NL}^{(i)}$ denote the LoS and non-LoS path-loss exponents associated with the i-th air-ground link, respectively. $\chi_L^{(i)}$ is the LoS occurrence probability, given by

$$\chi_L^{(i)} = \frac{1}{1 + c_1\exp(c_1c_2 - c_2\theta_i)}. \quad (30)$$

For the FA-enabled receiver, the spatial correlation among antenna ports is modeled using the more realistic Jake's correlation model. Specifically, the (k_1, k_2)-th element of the correlation matrix $\mathbf{J}$ is given by

$$[\mathbf{J}]_{k_1,k_2} = J_0\left(\frac{2\pi W|k_1-k_2|}{N-1}\right). \quad (31)$$

In Fig. 5, we plot the success probability versus θ_1, i.e., Alice-UAV link elevation angle, where the interferer lies on the line segment connecting Alice and the UAV ground projection. Other simulation parameters are summarized in Table I. The

[5] As a rough engineering reference, consider a typical micro-cell base-station transmit power of 33 dBm. Based on the representative parameter settings listed in Table I, the resulting P_j is on the range of 25–30 dB.

TABLE I: Simulation Parameters (cf. [17]).

Parameter	Value
Transmit powers	$P_a = P_j = 33$ dBm
System bandwidth	20 MHz
Noise power density	-174 dBm/Hz
Terrestrial path-loss exponent	3.5
Alice-Bob / Interferer-Bob distances	$d_{AB} = d_{JB} = 100$ m
Nakagami-m parameters	$c_1 = 1$, $c_2 = 2\ln(100)/\pi$
Air-ground path-loss exponents	$\alpha_L = 2$, $\alpha_{NL} = 3.5$
Alice-UAV distance	$D_1 = 300$ m
Alice-interferer distance	$d_{AJ} = 200$ m

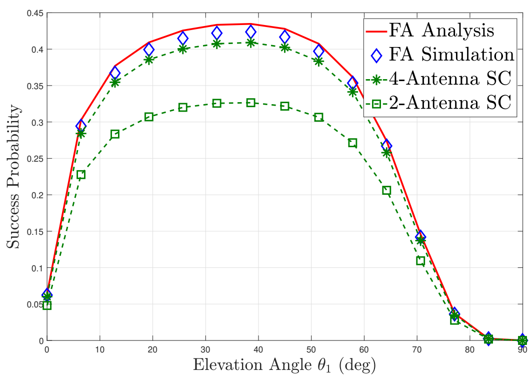

Fig. 5: $P_{\rm suc}$ versus θ_1 for $W = 1$, $N = 16$ and optimized ζ for COP.

red solid line represents the analytical results obtained from Corollary 2, which closely match the Monte Carlo simulations, thereby confirming the accuracy of the developed analytical framework under the considered realistic conditions.[6] It can be observed that the success probability first increases with θ_1, reaches its maximum around $35°$–$40°$, and then gradually decreases as θ_1 approaches $90°$. This trend is mainly caused by the different variations of the Alice-UAV and interferer-UAV links. As θ_1 increases, the LoS probability of the Alice-UAV link becomes larger, making Alice's signal more detectable at the UAV. Meanwhile, θ_2 first increases and then decreases under the considered geometry, so the interference power received at the UAV exhibits a non-monotonic variation. It can be also observed that the proposed FA receiver consistently outperforms a conventional 4-antenna receiver employing selection combining (SC) [21], where the antenna with the highest instantaneous SINR is selected, making SC a natural benchmark under the single-RF-chain constraint.

VI. Conclusion

This paper investigated FA-assisted covert communications in the presence of terrestrial interference and an aerial UAV warden. Closed-form expressions were derived for the UAV detection performance. By extending an eigenvalue-based weighted approximation to interference-limited FA systems, a highly tractable OP expression at the legitimate receiver was obtained, avoiding complicated integral evaluations. Based on these results, the success probability of covert communications was analyzed. Numerical results demonstrated the effectiveness of FA in enhancing covert communications. Specifically, for a fixed FA size, increasing the number of FA ports continuously improves the covertness performance while reducing the required transmit power. The analytical framework was further shown to maintain high accuracy under both realistic propagation conditions and practical spatial correlation models.

[6]Since m_1 and m_2 are generally non-integers in (27), Lemma 1 is no longer applicable. Hence, $P_M(\zeta)$ is evaluated numerically from (15), whereas the OP at Bob is still obtained from Lemma 3.

References

[1] K.-F. Tong, B. Liu, and K.-K. Wong, "Designs and challenges in fluid antenna system hardware," *Electronics*, vol. 14, no. 7, 2025.

[2] H. Zhao and D. Slock, "Coded caching enabled fluid antenna multiple access for interference-free connectivity," *IEEE Trans. Wireless Commun.*, vol. 25, pp. 6301–6316, 2026.

[3] D. Ma, B. Liu, J. Yang, Y. Fang, T. Wu, and K.-F. Tong, "Meta-fluid antenna-enabled multi-user ISAC: Architecture implementation, algorithm design, and full-wave validation," *IEEE J. Sel. Topics Signal Process.*, vol. 20, no. 3, pp. 247–261, 2026.

[4] X. Chen, J. An, Z. Xiong, C. Xing, N. Zhao, F. R. Yu, and A. Nallanathan, "Covert communications: A comprehensive survey," *IEEE Commun. Surv. Tutor.*, vol. 25, no. 2, pp. 1173–1198, 2023.

[5] F. Yang, X. Qin, S. Gong, N. Deng, C. Xing, and N. Zhao, "A survey of covert UAV communications," *Chin. J. Aeronaut.*, vol. 38, no. 10, p. 103493, 2025.

[6] J. Yao, L. Xin, T. Wu, M. Jin, K.-K. Wong, C. Yuen, and H. Shin, "FAS for secure and covert communications," *IEEE Internet Things J.*, vol. 12, no. 11, pp. 18 414–18 418, Jun. 2025.

[7] F. R. Ghadi, M. Kaveh, R. Jantti, and F. J. Lopez-Martinez, "On performance of FAS-aided covert communications," in *Proc. IEEE Veh. Technol. Conf. (VTC) Spring*, 2025.

[8] M. Khammassi, A. Kammoun, and M.-S. Alouini, "A new analytical approximation of the fluid antenna system channel," *IEEE Trans. Wireless Commun.*, vol. 22, no. 12, pp. 8843–8858, Dec. 2023.

[9] W. K. New, K.-K. Wong, H. Xu, K.-F. Tong and C.-B. Chae, "Fluid antenna system: New insights on outage probability and diversity gain," *IEEE Trans. Wireless Commun.*, vol. 23, no. 1, pp. 128–140, Jan. 2024.

[10] J. D. Vega-Sánchez, A. E. López-Ramírez, L. Urquiza-Aguiar, and D. P. M. Osorio, "Novel expressions for the outage probability and diversity gains in fluid antenna system," *IEEE Wireless Commun. Lett.*, vol. 13, no. 2, pp. 372–376, Feb. 2024.

[11] H. Zhao and D. Slock, "Analytical insights into outage probability and ergodic capacity of fluid antenna systems," *IEEE Wireless Commun. Lett.*, vol. 14, no. 5, pp. 1581–1585, May 2025.

[12] K.-K. Wong and K.-F. Tong, "Fluid antenna multiple access," *IEEE Trans. Wireless Commun.*, vol. 21, no. 7, pp. 4801–4815, Jul. 2022.

[13] K.-K. Wong, D. Morales-Jimenez, K.-F. Tong, and C.-B. Chae, "Slow fluid antenna multiple access," *IEEE Trans. Commun.*, vol. 71, no. 5, pp. 2831–2846, May 2023.

[14] H. Xu, K.-K. Wong, W. K. New, K.-F. Tong, Y. Zhang, and C.-B. Chae, "Revisiting outage probability analysis for two-user fluid antenna multiple access system," *IEEE Trans. Wireless Commun.*, vol. 23, no. 8, pp. 9534–9548, Aug. 2024.

[15] P. Ramírez-Espinosa, D. Morales-Jimenez, and K.-K. Wong, "A new spatial block-correlation model for fluid antenna systems," *IEEE Trans. Wireless Commun.*, vol. 23, no. 11, pp. 15 829–15 843, Nov. 2024.

[16] H. Zhao and D. Slock, "Fluid antenna port selection in underlay cognitive radio networks," in *Proc. 7th Comput., Commun. IoT Appl. Conf. (ComComAp)*, Dec 2025.

[17] P. Kumar and S. Majhi, "UAV-assisted network coded cooperation by using height-dependency shaping parameters in Nakagami-m faded channel," *IEEE Access*, vol. 12, pp. 11 688–11 699, 2024.

[18] I. S. Gradshteyn and I. M. Ryzhik, *Table of integrals, series, and products*, 7th ed. Academic press, 2007.

[19] F. R. Ghadi, K.-K. Wong, M. Kaveh, H. Xu, W. Kiat New, F. Javier López-Martínez, and H. Shin, "Fluid antenna multiple access with simultaneous non-unique decoding in strong interference channel," *IEEE Trans. Wireless Commun.*, vol. 24, no. 12, pp. 10 183–10 195, Dec. 2025.

[20] K.-K. Wong, K.-F. Tong, Y. Chen, and Y. Zhang, "Closed-form expressions for spatial correlation parameters for performance analysis of fluid antenna systems," *Electron. Lett.*, vol. 58, no. 11, pp. 454–457, 2022.

[21] H. Zhao *et al.*, "Secrecy outage on transmit antenna selection/maximal ratio combining in MIMO cognitive radio networks," *IEEE Trans. Veh. Technol.*, vol. 65, no. 12, pp. 10 236–10 242, 2016.